The International Journal of Advanced Manufacturing Technology (2019) 105:3289–3302
https://doi.org/10.1007/s00170-019-04508-1

ORIGINAL ARTICLE

A review of basic crystallography and x-ray diffraction applications

E. S. Ameh [1]

Received: 7 June 2019 / Accepted: 24 September 2019 / Published online: 12 November 2019

Abstract
Although various researched works have been carried out in x-ray crystallography and its applications, but there are still limited number of researches on crystallographic theories and industrial application of x-ray diffraction. The present study reviewed and provided detailed discussion on atomic arrangement of single crystals, mathematical concept of Bravais, reciprocal lattice, and application of x-ray diffraction. Determination of phase identification, crystal structure, dislocation density, crystallographic orientation, and gran size using x-ray diffraction peak intensity, peak position, and peak width were discussed. The detailed review of crystallographic theories and x-ray diffraction application would benefit majorly engineers and specialists in chemical, mining, iron, and steel industries.

Keywords Crystal structure · Crystallography · Intensity · Lattice · Unit cell · X-ray diffraction

1 Introduction

Atoms in materials are arranged into crystal structures and microstructures [1]. Periodic arrangement of atoms depends strongly on external factors such as temperature, pressure, and cooling rate during solidification. Solid elements and their compounds are classified into amorphous, polycrystalline, and single crystalline materials [2]. The amorphous solid materials are isotropic in nature because their atomic arrangements are not regular and possess the same properties in all directions. In contrast, the crystalline materials are anisotropic because their atoms are arranged in regular and repeated pattern, and their properties vary with direction [3]. The polycrystalline materials are combinations of several crystals of varying shapes and sizes. The properties of polycrystalline materials are strongly dependent on distribution of crystals sizes, shapes, and orientations within the individual crystal [4]. About 95% of most solid materials are crystalline in nature, and the international center diffraction data (ICDD) maintain about 50,000 inorganics and 25,000 organic crystalline and single component databases [5]. Diffraction pattern or intensities of x-ray diffraction techniques are used for characterizing and probing arrangement of atoms in each unit cell, position of atoms, and atomic spacing angles because of comparative wavelength of x-ray to atomic size [6]. The x-ray diffraction, which is a non-destructive technique, has wide range of material analysis including minerals, metals, polymers, ceramics, plastics, semiconductors, and solar cells [7]. The technique also has wide industry application including aerospace, power generation, microelectronics, and several others [8].

Hart [9] carried out review on comparative methods of measuring Bragg's angle based on crystal arrangement and general principle. Fewster [10] highlighted techniques of lattice parameter measurement and concluded that the most suitable method depends strongly on materials crystals. Magner et al. [11] gave historical review of retained austenite measurement using x-ray. Guidelines to measure single crystal with over 200 μm dimension as well as procedure to measure lattice spacing was highlighted by Jesche et al. [12]. A review of x-ray diffraction relating to x-ray powder method and the mechanism was provided by Toraya [13]. Zhengi et al. [14] proposed a concept for crystal orientation measurement using butterfly diagram obtained from powder x-ray diffraction. The new concept gave direct information on single crystals and polycrystals orientations. A technical review of x-ray technique in terms of nanomaterial characterization and applications was conducted by Sharma et al [5]. The x-ray crystallography remained a complex field of study despite wide industrial applications. Several literatures have focused on practical applications of x-ray diffraction and rarely has technical review of crystal structures, and x-diffraction applications theories been conducted. Crystallography is taken as a course at tertiary institutions and training courses. Nonetheless, many

✉ E. S. Ameh
stanley.ameh@yahoo.com

[1] Department of Mechanical Engineering, University of Benin, Benin, Edo State, Nigeria

student and engineers have not fully understood the basic of crystal structure and x-ray crystallography. This article provides technical review with systematic explanation of basic crystal structure and x-ray diffraction to provide self-explanation.

2 Crystal structure

In crystalline structures, arrays of atoms are arranged in a regular and repeated pattern. But the smallest repeating element in the crystal is called a unit cell. In three dimensions, the shape and size of the unit cell (Fig. 1) can be described by length of three axes (a, b, c) and the angles between the axes [5]. The arrays of atoms are orderly arranged by pure translation (transformation) without change in rotation or orientation but change of atoms position. The translation maybe in three dimensions, two dimensions, and one dimension [15]. A lattice is a periodic arrangement of points collection in a crystal, and these lattices can be represented by set of translation vectors in both three and two dimensions as demonstrated in Fig. 2 a and b, respectively.

Bravais introduced a mathematical concept called space lattice in 1848 to describe crystal structure arrangement (Fig. 3). The space lattice defines infinite number of points in space such that the point arrangement around a point is identical around any other points [17]. The axes x, y, z system (Fig. 1) is used to designate points arrangement in space lattice. All possible arrangement of points in lattice space in three-dimensions can be represented by 14 lattices (Fig. 3), while the 14 Bravais lattices is classified into 7 crystal system (Table 1) based on the length of the axes, angles between them, and symmetry properties.

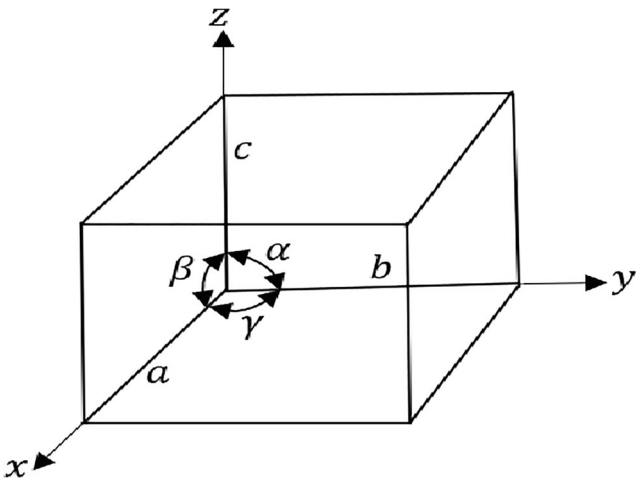

Fig. 1 Three-dimension unit cell vector [2]

2.1 Symmetry operation

Symmetry is defined as certain shape or arrangement of an object. A structure of crystal is said to be symmetrical if certain direction of geometry and physical property of crystal are reproduced by certain operation [18]. There are 230 different repetitive patterns of atomic elements that can be arranged to form actual crystal structure. However, all the crystals have been classified into 7 crystal system based on n-fold rotation, reflection, inversion center and rotation-inversion symmetry operation. Further combination of three symmetry operations results in 32 crystal symmetry classes point group [18, 19]. The n-fold rotation (Fig. 4) means rotation about an imaginary axis through angles $360^{\circ}/n$ reproduces the same object and denoted with symbol (n = 1, 2, 3, 4, 5, 6) . Where, n is the number of allowed repetitions in 360° rotation, but n = 1 means no symmetry [21]. A reflection symmetry (Fig. 5) is a plane reflection where arrangement of each point in the crystal reproduces mirror image on left and right sides of the plane, and it is denoted with symbol m [2]. Invasion is a type of symmetry operation where a point in the lattice exist such that inversion through the point reproduces an identical arrangement, but in opposite direction and is denoted with p symbol [4]. Whereas the rotation-inversion symmetry operation (Fig. 6) is a combination of rotation and inversion denoted as $\overline{n}$ [20]. Additionally, there is a translation symmetry where movement along three-dimensional space creates repeated structure and only occurs in solid state. The translational symmetry element is further divided into glide and screw symmetries. The glide plane is a combination of translation and reflection symmetry operation while the screw axis is a combination of translation and rotation symmetry operations [20, 21]. All the symmetries are classified into point group and space group. The point group is the symmetry elements without translation while space group is symmetry element with translation [19].

2.2 Bravais and reciprocal lattices

A Bravais lattice is a set of lattice points with position vectors $\boldsymbol{R}$, while reciprocal lattice is a set of vectors, $\boldsymbol{K}$ that gives plane wave with periodicity of Bravais lattice. The lattice position vectors ($\boldsymbol{R}$) and reciprocal lattice vectors ($\boldsymbol{K}$) are given as [22, 23]:

$$\boldsymbol{R} = n_1\boldsymbol{a_1} + n_2\boldsymbol{a_2} + n_3\boldsymbol{a_3} \tag{1}$$

$$\boldsymbol{K} = h\boldsymbol{b_1} + k\boldsymbol{b_2}\, l\boldsymbol{b_3} \tag{2}$$

where, n_1, n_2, n_3 are integers; h, k, l are miller indices of plane perpendicular to the reciprocal lattice vectors; $\boldsymbol{a_1}$,$\boldsymbol{a_2}$, $\boldsymbol{a_3}$ are primitive lattice vectors for the position vector and $\boldsymbol{b_1}$, $\boldsymbol{b_2}$, $\boldsymbol{b_3}$ are primitive lattice vectors for reciprocal vector. Since the vector $\boldsymbol{K}$ belong to the reciprocal lattice of Bravais lattice with point position vector $\boldsymbol{R}$, yield relationship of [22]:

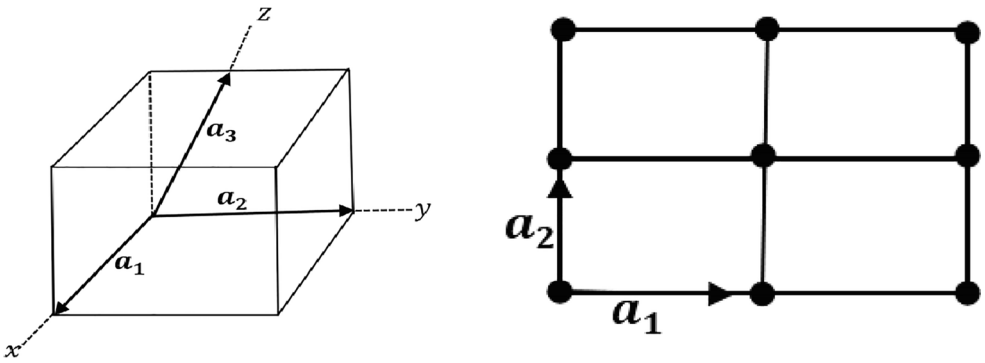

Fig. 2 **a** Three-dimension lattice with translation [2]. **b** Two-dimension lattice with translation vector [2]

$$e^{iK\cdot(r+R)} = e^{iK\cdot r} \tag{3}$$

or

$$e^{iK\cdot R}=1 \tag{4}$$

Equations (3–4) are satisfied if $\boldsymbol{K.R}=2\pi n$ and, therefore, can been rewritten as follows:

$$(h\boldsymbol{b_1} + k\boldsymbol{b_2}\ l\boldsymbol{b_3})\cdot(n_1\boldsymbol{a_1} + n_2\boldsymbol{a_2} + n_3\boldsymbol{a_3}) = 2\pi n, \textit{with n an integer}\cdot \tag{5}$$

The primitive vectors $\boldsymbol{b_1}$, $\boldsymbol{b_2}$, $\boldsymbol{b_3}$ from the reciprocal lattice are given as follows:

$$\frac{\boldsymbol{b_1}=2\pi\boldsymbol{a_2}\times\boldsymbol{a_3}}{\boldsymbol{a_1}.(\boldsymbol{a_2}\times\boldsymbol{a_3})} \tag{6}$$

$$\frac{\boldsymbol{b_2}=2\pi\boldsymbol{a_3}\times\boldsymbol{a_1}}{\boldsymbol{a_1}.(\boldsymbol{a_2}\times\boldsymbol{a_3})} \tag{7}$$

$$\frac{\boldsymbol{b_3}=2\pi\boldsymbol{a_1}\times\boldsymbol{a_2}}{\boldsymbol{a_1}.(\boldsymbol{a_2}\times\boldsymbol{a_3})} \tag{8}$$

From Eqs. (6–8), it is easy to derive Eq. (9):

$$\boldsymbol{a_i}\cdot\boldsymbol{b_j}=2\pi\delta_{ij} \tag{9}$$

where, $\boldsymbol{a_i}$ are primitive lattice vectors of the position vectors; $\boldsymbol{b_j}$ are primitive lattice vectors of reciprocal vectors and δ_{ij} are lattice tensor.

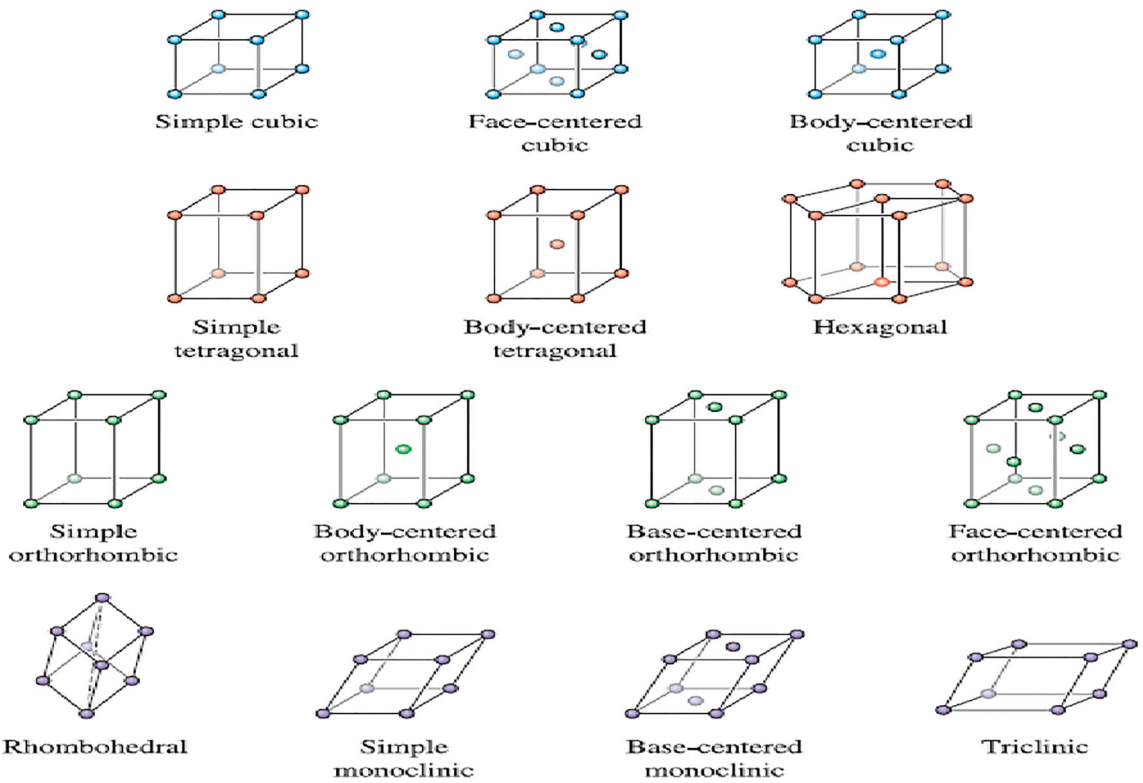

Fig. 3 The 14 types of Bravais lattices [16]

Table 1 The 7-crystal system [18]

System	Unit cell characteristic	Bravias lattice	Symmetry
Cubic	$a=b=c$ $\alpha=\beta=\gamma\neq 90^0$	Simple Body-centered Face-centered	4 3-fold rotation axes
Triclinic	$a\neq b\neq c$ $\alpha\neq\beta\neq\gamma$	Simple	No plane and no axes
Monoclinic	$a\neq b\neq c$ $\alpha=\beta=90^0\neq\gamma$	Simple Base-centered	1 2-fold rotation axes or one plane
Orthorhombic	$a\neq b\neq c$ $\alpha=\beta=\gamma=90^0$	Simple Base-centered Body-centered Face-centered	3 mutually perpendicular 2-fold rotation axes, or 2 planes intersecting in a 2-fold axis
Tetragonal	$a=b\neq c$ $\alpha=\beta=\gamma=90^0$	Simple Body-centered	1 4-fold rotation axes or a 4-fold rotation inversion axes
Hexagonal	$a=b\neq c$ $\alpha=\beta=90^0$, $\gamma=120^0$	Simple	1 6-fold rotation axes
Trigonal	$a=b=c$ $\alpha=\beta=\gamma\neq 90^0$	Simple	1 3-fold rotation axes

Proving Eq. (9) is by multiplying Eqs. (6–8) by $\boldsymbol{a_1}$:

$$\boldsymbol{a_1}.\boldsymbol{b_1}=2\pi\frac{\boldsymbol{a_1}.(\boldsymbol{a_2}\times\boldsymbol{a_3})}{\boldsymbol{a_1}.(\boldsymbol{a_2}\times\boldsymbol{a_3})}=2\pi \tag{10}$$

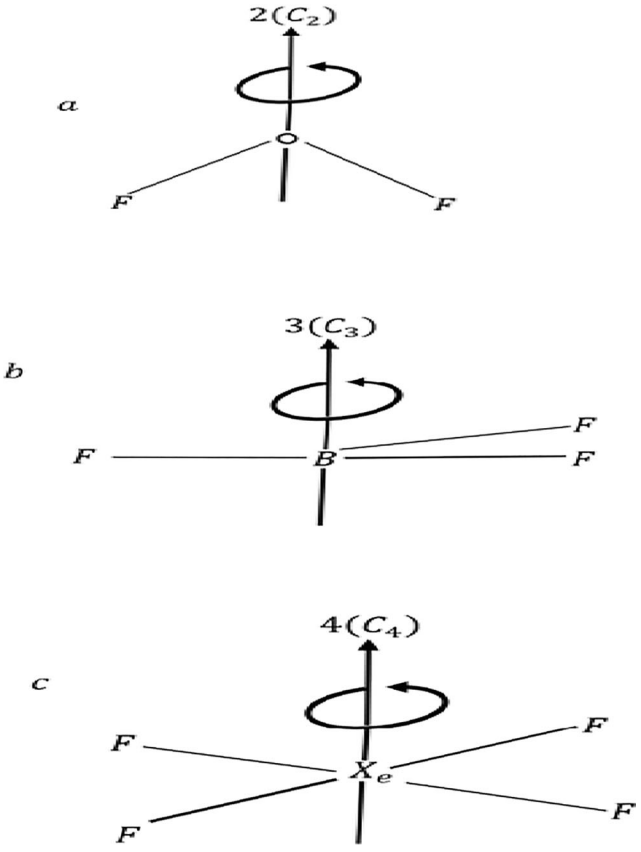

Fig. 4 Typical rotation symmetry in crystal structure **a** 2-fold axis, **b** 3-fold axis, **c** 4 fold axis [20]

$$\boldsymbol{a_1}.\boldsymbol{b_2}=2\pi\frac{\boldsymbol{a_1}.(\boldsymbol{a_3}\times\boldsymbol{a_1})}{\boldsymbol{a_1}.(\boldsymbol{a_2}\times\boldsymbol{a_3})}=0 \tag{11}$$

$$\boldsymbol{a_1}.\boldsymbol{b_3}=2\pi\frac{\boldsymbol{a_1}.(\boldsymbol{a_1}\times\boldsymbol{a_2})}{\boldsymbol{a_1}.(\boldsymbol{a_2}\times\boldsymbol{a_3})}=0 \tag{12}$$

Two crystallographic planes that are perpendicular equal zero. Therefore, Eqs. (11–12) are equal to zero because the cross product of two vectors is perpendicular to both vectors.

2.3 Crystal distances and angles

Computations of angles help to determine the coordinate of each atom while computation of distance between atoms determines bond strength of atoms that are chemically bonded together. Computation of crystallographic distances and angles in crystal structure are carried out in lattice position space, reciprocal space, or both spaces [24, 25]. Two crystallographic directions given as $[u_1, v_1, w_1]$ and $[u_2, v_2, w_2]$ can be presented in lattice position vectors form [26]:

$$\boldsymbol{r_1}=u_1\boldsymbol{a_1}+v_1\boldsymbol{a_2}+w_1\boldsymbol{a_3} \tag{13}$$

$$\boldsymbol{r_2}=u_2\boldsymbol{a_1}+v_2\boldsymbol{a_2}+w_2\boldsymbol{a_3} \tag{14}$$

In lattice position space, the angle between two vectors $\boldsymbol{r_1}$ and $\boldsymbol{r_2}$ is given as:

$$\cos\alpha=\frac{\boldsymbol{r_1}\cdot\boldsymbol{r_2}}{|\boldsymbol{r_1}|\cdot|\boldsymbol{r_2}|}$$

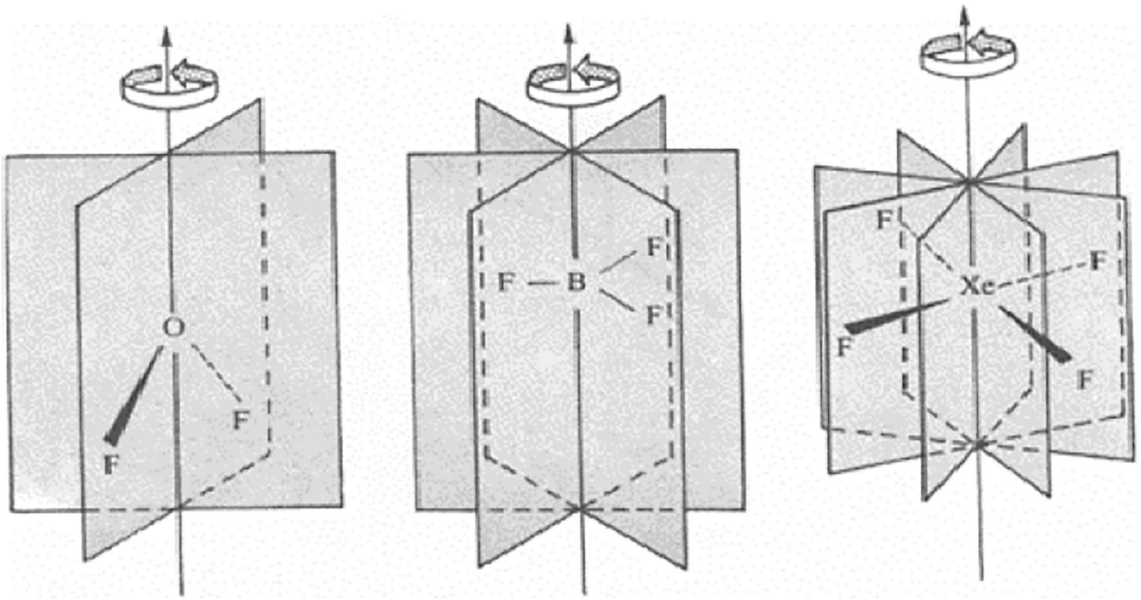

Fig. 5 Reflection plane symmetry of different structures [20]

$$= \frac{(u_1\boldsymbol{a_1} + v_1\boldsymbol{a_2} + w_1\boldsymbol{a_3}) \cdot (u_2\boldsymbol{a_1} + v_2\boldsymbol{a_2} + w_2\boldsymbol{a_3})}{\sqrt{(u_1\boldsymbol{a_1} + v_1\boldsymbol{a_2} + w_1\boldsymbol{a_3}) \cdot (u_1\boldsymbol{a_1} + v_1\boldsymbol{a_2} + w_1\boldsymbol{a_3})}\sqrt{(u_2\boldsymbol{a_1} + v_2\boldsymbol{a_2} + w_2\boldsymbol{a_3}) \cdot (u_2\boldsymbol{a_1} + v_2\boldsymbol{a_2} + w_2\boldsymbol{a_3})}} \tag{15}$$

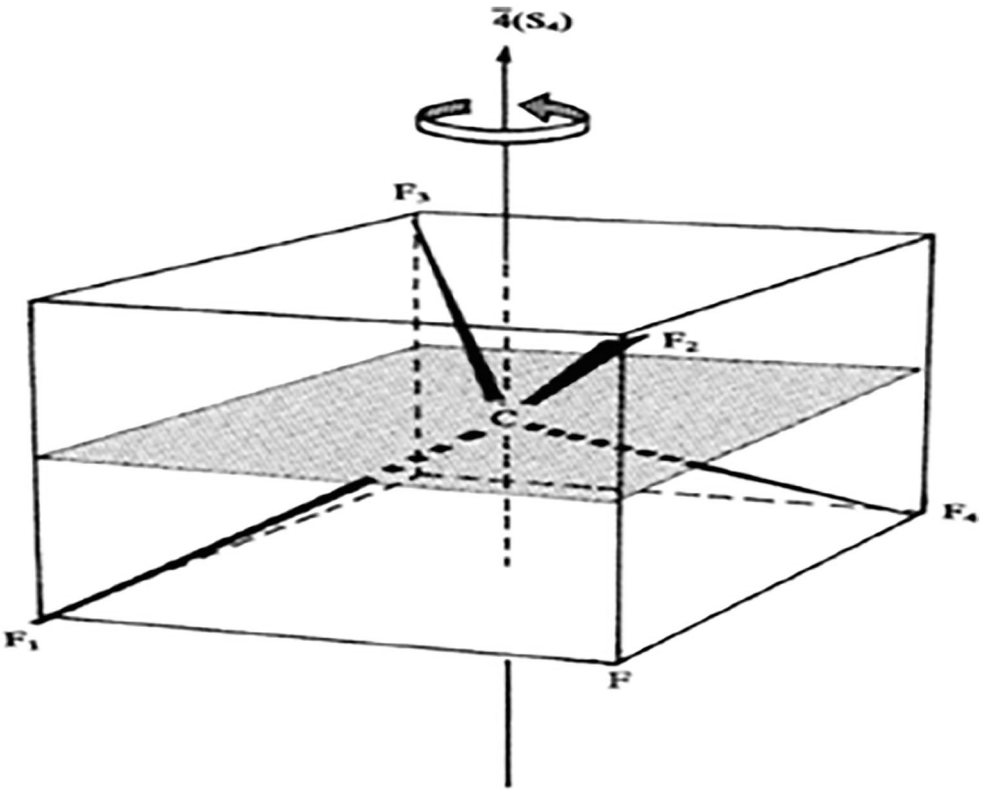

Fig. 6 The $\bar{4}$ rotations—inversion symmetry in tetrahedral molecule [20]

where, $|\boldsymbol{a_1}| = a$, $|\boldsymbol{a_2}| = b$, $|\boldsymbol{a_3}| = c$ for cubic, tetragonal, and orthorhombic crystals whose angles between translation vectors is 90° further reduces Eq. (15) to:

$$\cos\alpha = \frac{u_1u_2a^2 + v_1v_2b^2 + w_1w_2c^2}{\sqrt{(u_1a)^2 + (v_1b)^2 + (w_1c)^2}\sqrt{(u_2a)^2 + (v_2b)^2 + (w_2c)^2}} \tag{16}$$

In lattice position space, distance between two atoms in (x_1, y_1, z_1) and (x_2, y_2, z_2) in space is given as:

$$L = \sqrt{[(x_2-x_1)\boldsymbol{a_1}+(y_2-y_1)\boldsymbol{a_2} + (z_2-z_1)\boldsymbol{a_3}]} \cdot \sqrt{[(x_2-x_1)\boldsymbol{a_1}+(y_2-y_1)\boldsymbol{a_2} + (z_2-z_1)\boldsymbol{a_3}]} \tag{17}$$

Similarly, when angles between translation vectors are 90° and where, $|\boldsymbol{a_1}| = a$, $|\boldsymbol{a_2}| = b$, $|\boldsymbol{a_3}| = c$, equation (17) can be rewritten as:

$$L = \sqrt{(x_2-x_1)^2a^2 + (y_2-y_1)^2b^2 + (z_2-z_1)^2c^2} \tag{18}$$

In the same manner, two crystallographic planes given as (h_1, k_1, l_1) and (h_2, k_2, l_2) can be represented in reciprocal lattice vector form as [26]:

$$\boldsymbol{K_1} = h_1\boldsymbol{b_1} + k_1\boldsymbol{b_2} + l_1\boldsymbol{b_3} \tag{19}$$

$$\boldsymbol{K_2} = h_2\boldsymbol{b_1} + k_2\boldsymbol{b_2} + l_2\boldsymbol{b_3} \tag{20}$$

In lattice reciprocal space, the angles between two vectors in crystallographic planes is given as:

$$\cos\alpha = \frac{\boldsymbol{K_1}\cdot\boldsymbol{K_2}}{|\boldsymbol{K_1}|\cdot|\boldsymbol{K_2}|}$$

$$= \frac{(h_1\boldsymbol{b_1} + k_1\boldsymbol{b_2} + l_1\boldsymbol{b_3}).(h_2\boldsymbol{b_1} + k_2\boldsymbol{b_2} + l_2\boldsymbol{b_3})}{\sqrt{(h_1\boldsymbol{b_1} + k_1\boldsymbol{b_2} + l_1\boldsymbol{b_3})(h_1\boldsymbol{b_1} + k_1\boldsymbol{b_2} + l_1\boldsymbol{b_3})}\sqrt{(h_2\boldsymbol{b_1} + k_2\boldsymbol{b_2} + l_2\boldsymbol{b_3})(h_2\boldsymbol{b_1} + k_2\boldsymbol{b_2} + l_2\boldsymbol{b_3})}} \tag{21}$$

When angles between translation vectors in reciprocal space is 90° and $|\boldsymbol{b_1}| = {}^1/_a$, $|\boldsymbol{b_2}| = {}^1/_b$, $|\boldsymbol{b_3}| = {}^1/_c$, Eq. (21) is reduced to:

$$\cos\alpha = \frac{h_1h_2/a^2 + k_1k_2/b^2 + l_1l_2/c^2}{\sqrt{(h_1/a)^2 + (k_1/b)^2 + (l_1/c)^2}\sqrt{(h_2/a)^2 + (k_2/b)^2 + (l_2/c)^2}} \tag{22}$$

Calculation of vectors length $\boldsymbol{K_2}$ in reciprocal lattice space for crystallographic planes (h, k, l) is the same way of calculating d-spacing, which vary with different crystals. To calculate angle between crystallographic plane vector $\boldsymbol{K_1}$ (h, k, l) and crystallographic direction vector, $\boldsymbol{r_1}$ (u, v, w) is performed using both position and reciprocal spaces:

$$\cos\alpha = \frac{\boldsymbol{r_1}\cdot\boldsymbol{K_1}}{|\boldsymbol{r_1}|\cdot|\boldsymbol{K_1}|}$$

$$= \frac{(u_1\boldsymbol{a_1} + v_1\boldsymbol{a_2} + w_1\boldsymbol{a_3})\cdot(h_1\boldsymbol{b_1} + k_1\boldsymbol{b_2} + l_1\boldsymbol{b_3})}{\sqrt{(u_1\boldsymbol{a_1} + v_1\boldsymbol{a_2} + w_1\boldsymbol{a_3})\cdot(u_1\boldsymbol{a_1} + v_1\boldsymbol{a_2} + w_1\boldsymbol{a_3})}\sqrt{(h_1\boldsymbol{b_1} + k_1\boldsymbol{b_2} + l_1\boldsymbol{b_3})(h_1\boldsymbol{b_1} + k_1\boldsymbol{b_2} + l_1\boldsymbol{b_3})}} \tag{23}$$

When the angle between vectors is 90° and setting $u_1 = h_1$, $v_1 = k_1$ and $w_1 = l_1$ if the two vectors have the same indices reduce Eq. (23) to:

$$\cos\alpha = \frac{h_1^2 + k_1^2 + l_1^2}{\sqrt{(h_1\boldsymbol{a_1} + k_1\boldsymbol{a_2} + l_1\boldsymbol{a_3})\cdot(h_1\boldsymbol{a_1} + k_1\boldsymbol{a_2} + l_1\boldsymbol{a_3})}\sqrt{(h_1\boldsymbol{b_1} + k_1\boldsymbol{b_2} + l_1\boldsymbol{b_3})(h_1\boldsymbol{b_1} + k_1\boldsymbol{b_2} + l_1\boldsymbol{b_3})}} \tag{24}$$

Equation (24) can be further reduced or transformed depending on the setting of $|\boldsymbol{a_1}|$, $|\boldsymbol{a_2}|$, $|\boldsymbol{a_3}|$, $|\boldsymbol{b_1}|$, $|\boldsymbol{b_2}|$, and $|\boldsymbol{b_3}|$ which are depended on type of crystal system.

2.4 Miller indices for planes

A set of coordinates expressed in the form of h, k, l that is defined by line from origin and cut through the axes (a, b, c) or axial vector ($\boldsymbol{a_1}, \boldsymbol{a_2}, \boldsymbol{a_3}$) is called miller indices for that set of lattice planes [27]. The miller indices are used to express lattice planes and to specify orientation of planes in space and not position. The letter h, k, l are miller indices for planes and are designated in curvilinear bracket as (h, k, l). Crystallographic planes are equivalent to each other by symmetry if the atomic d-spacing along each plane is the same. Therefore, cubic front and back faces which intercept the x-axis and parallel to y- and z-axes, yield miller indices (100); the top and bottom faces, which intercept the z-axis and parallel to x- and y-axis is (001). Similarly, the left and right faces of cubic crystal intercept the y-axis and parallel to both x- and z-axes have (010). Consequently, a zero miller index implies that the plane (face) is parallel to corresponding unit cell axis and at infinity [17, 25]. The equivalent planes is called family or form of indices and represented as follows: {100 = (100), (010), (001), (100), (010), (001). A simple procedure for finding the miller indices for any given plane of atoms within a crystal is as follows [18]:

- Set up coordinate axes (x, y, z) along the angles of the unit cell.
- Identify the coordinates at which the crystallographic plane intersects the x-, y-, and z-axes.
- Take intercept along axis to be infinity (zero value) if crystallographic plane is parallel to the axis.
- Consider having family of plane or moving origin of coordinates to a lattice point not on the plane to be indexed because miller indices cannot be established for plane passing through origin of coordinates.
- Record the intercept components in x, y, z order
- Multiply the intercept components by the smallest possible set of whole number.
- Enclose the whole number set in curvilinear bracket and place bars over negative indices.

2.5 Miller indices for direction

Crystallographic directions are used to show orientation of a single crystal or polycrystalline materials. Magnetic properties of iron including other magnetic materials depend strongly on crystallographic direction. For example, iron [100] direction is easier to magnetize than the one with [111] and [1100] directions [16]. Three indices (u, v, w) are employed in specifying crystallographic directions in the x, y, z directions, which are usually enclosed in square bracket as [u, v, w], but sometimes represented as [h, k, l]. Again, all parallel direction vectors have the same direction indices. Thus, miller indices direction of x-axis is [100]; the y-axis is [010] and z-axis has [001] for cubic crystal [17]. When atomic spacing along each direction is the same, the direction is equivalent. The equivalent direction is called family or form indices. In the case of cubic crystal, crystallographic equivalent directions are given as [28]:

⟨100⟩= [100], [010], [001], [010], [001], [100]

The miller indices for crystallographic direction can be established using the following procedure [29]:

- Set up coordinate axes (x, y, z) along the angles of the unit cell.
- Draw up vector of arbitrary length in the direction of interest and define the detail as the origin.
- Decompose or resolve the drawn vector into it component vectors ($\boldsymbol{a_1}, \boldsymbol{a_2}, \boldsymbol{a_3}$) along each of the coordinate axes (x, y, z).
- Record the vector components in x, y, z order.
- Multiply the component by the smallest set of whole number.
- Enclose the whole number set in square bracket and place bars over negative indices.
- Recognize that a plane and the direction normal to the plane of cubic crystal have the same miller indices as [110] direction that is normal to the (110) planes.

3 X-ray diffraction principle

When x-ray impinges upon atoms of solid, the x-rays are scattered by the electrons in the atoms. Either constructive or destructive waves interference occurs along different direction as the scattered waves (diffraction pattern) are emitted by atoms at different positions [1]. However, constructive interference occurs if the solid has orderly arrangement of atomic structure. A strong relationship between diffraction patterns and periodic atomic structure of crystals in materials exist. Atomic arrangement (periodicity) with long repeated distances causes diffraction at small angles whereas short repeated distances lead to diffraction at high angles [1]. Diffraction peak position is used to determine shape and size of unit cell while diffraction peak intensity determines atomic position within the cell and atomic number [30].

3.1 Bragg's theory

Bragg provided simple alternative explanation and measurement for diffraction of monochromatic x-ray from single crystal after Laue discovery of the x-ray diffraction [31]. The Bragg's analysis (Fig. 7 a) assumed that crystals are in layers or atomic planes (lattice plane- *hkl*) are in layers with spacing distance, *d* and produce reflection when incident light or x-ray impinges on the planes of atoms [32]. Secondly, incident beam makes equal angle with corresponding diffracted beam at the lattice plane. For constructive interference, the Bragg's diffraction condition is satisfied if the path difference lengths equal $n\lambda$, and Pythagoras theorem (Fig. 7 b) was used to derive Eq. (29).

According to the Bragg's law constructive interference occurs only if [32]:

$$\mathrm{AB} + \mathrm{BC} = n\lambda \tag{25}$$

From x-ray diffraction pattern schematics (Fig. 7 a), AB = BC, therefore:

$$n\lambda = 2\mathrm{AB} \tag{26}$$

Representing ΔABZ (Fig. 7 b) from diffraction pattern schematic (Fig. 7a) for Pythagoras theorem derivation yield:

$$\sin\theta = \frac{\mathrm{AB}}{d} \tag{27}$$

$$\mathrm{AB} = d\sin\theta \tag{28}$$

$$n\lambda = 2d\sin\theta \tag{29}$$

where, λ= x-ray wavelength, *n*= order of reflection, *d*= spacing distance and *θ*= angle of diffraction beam. Since *n* is the order of diffraction (reflection) from set of lattice planes (*hkl*) with interplanar spacing d_{hkl}:

$$d = \frac{d_{hkl}}{n} \tag{30}$$

Then, Eq. (29) can be rewritten by substituting into Eq. (30) as follows:

$$\lambda = 2d_{hkl}\sin\theta_{hkl} \tag{31}$$

The Bragg's law can be represented in vector notation along incident and diffracted beams' directions as shown in Fig. 8. Therefore, the Bragg's law in vector notation is expressed as [30]:

$$\frac{(\boldsymbol{S}-\boldsymbol{S}_o)}{\lambda} = \boldsymbol{d}^*_{hkl} = h\boldsymbol{a_1} + k\boldsymbol{a_2} + l\boldsymbol{a_3} \tag{32}$$

where, $\boldsymbol{S}$=unit vector along diffracted beam direction and $\boldsymbol{S}_o$=unit vector along incident beam direction.

3.2 Laue theory

Ewald theory leads to the discovery of x-ray diffraction by Laue, but that theory was rarely needed in the study of crystal structure [31]. Laue analysis assumed crystal as buildup of rows of atoms along *x*-axis, *y*-axis, and *z*-axis in three dimensions. Supposing, AB (Fig. 9a) is a wave crest of incident beam and *CD* is the wave crest of diffracted beam for constructive interference for waves from atoms along *z*-axis [17, 25]. According to Putnam et al. [15], if diffracted path difference corresponds to integer (whole) number of incident beam wavelength, then the diffracted beam undergoes constructive interference (in-phase). However, if diffracted beams undergo destructive interference (out-of-phase), then incident beams do not correspond to wavelengths. Laue's law vector notation of the incident and diffracted beam directions and path difference between the diffracted beams are represented in Fig. 9b.

Mathematical representation of Laue first equation for path difference (AB − CD) corresponding to integer number of wavelength for a constructive interference is [25]:

$$(\mathrm{AB}-\mathrm{CD}) = a(\cos\alpha_n - \cos\alpha_0) = n_x\lambda \tag{33}$$

where, *a*=atom spacing along *x*-axis (or lattice parameter); α_n=angle of diffracted beam to *x*-axis; α_0= angle of incident

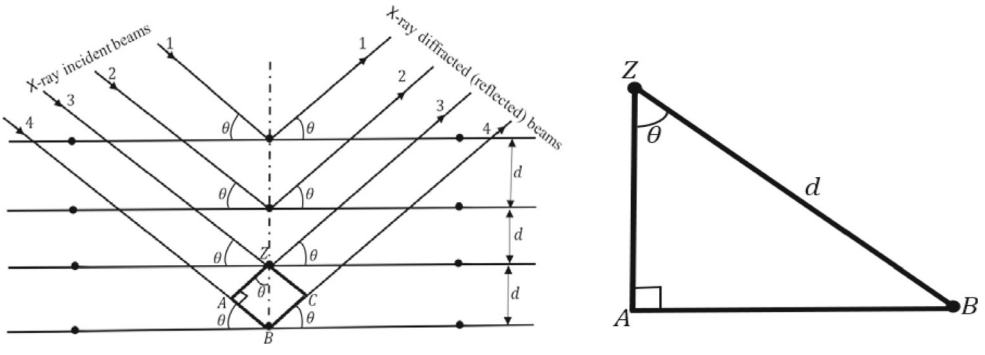

Fig. 7 **a** Schematic of x-ray diffraction pattern [32] **b** Pythagoras theorem [32]

a Schematic of x-ray diffraction pattern [32] **b** Pythagoras theorem [32]

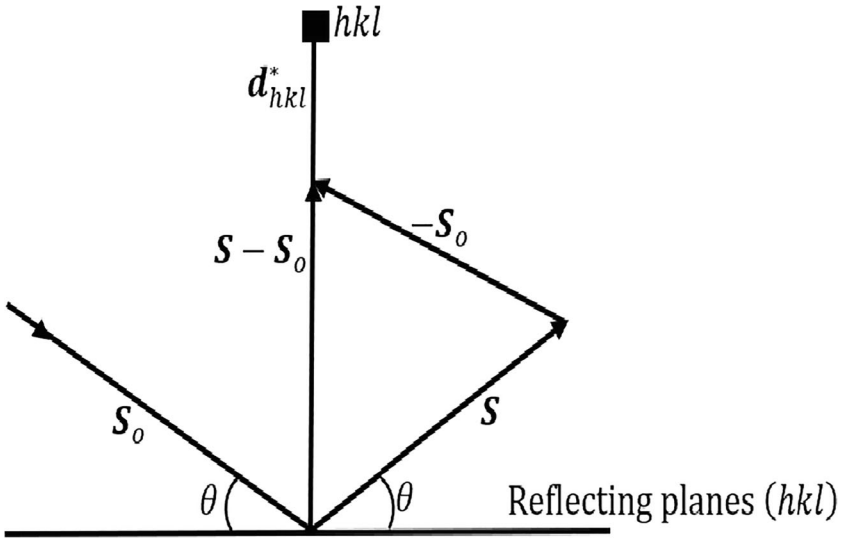

Fig. 8 Diagrammatic representation of Bragg's law in vector notation [25]

beam to x-axis and n_x=interger in order of diffraction. From Laue cones (Fig. 9b), Laue first equation (33) can be expressed in vector notation in x-axis as [25]:

$$a(\cos\alpha_n - \cos\alpha_0) = \boldsymbol{a_1}(\boldsymbol{S}-\boldsymbol{S}_o) = n_x\lambda \tag{34}$$

Since all the diffracted beams with the same path difference occur at the same angle to a row of atoms, the diffracted beams that fall on the row of atoms can be represented in three Laue cones (Fig. 10). Where, the three Laue cones' angles are α_0 (zero order, $n_x = 0$), α_1 (first order, $n_x = 1$), and α_2 (zero order, $n_x = 1$). Similarly, Laue second and third equations for row of atoms along y-axis and z-axis are given respectively as [25, 34]:

$$b(\cos\beta_n - \cos\beta_0) = \boldsymbol{a_2}(\boldsymbol{S}-\boldsymbol{S}_o) = n_y\lambda \tag{35}$$

$$c(\cos\gamma_n - \cos\gamma_0) = \boldsymbol{a_1}(\boldsymbol{S}-\boldsymbol{S}_o) = n_z\lambda \tag{36}$$

where, b and c are atom spacing along y-axis and z-axis respectively; β_n and β_0 are angle of diffracted and incident beams along y-axis respectively, and γ_n and γ_0 are angle of diffracted and incident beams along z-axis respectively. Indeed, practical application of Laue equations (34–36) is impossible because all the values in the equations cannot be determined for a given value of incident beam.

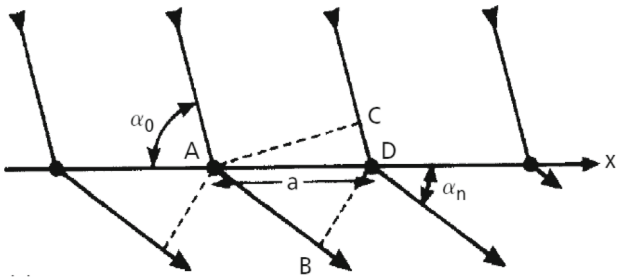

a Diffracted beams from row of atoms along x − axis[25].

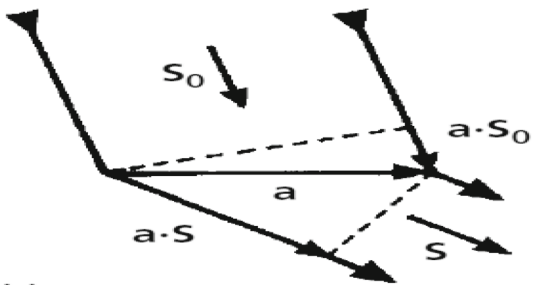

b Vector notation of incident diffraction beam direction and path difference [25]

Fig. 9 **a** Diffracted beams from row of atoms along x-axis [25]. **b** vector notation of incident diffraction beam direction and path difference [25]

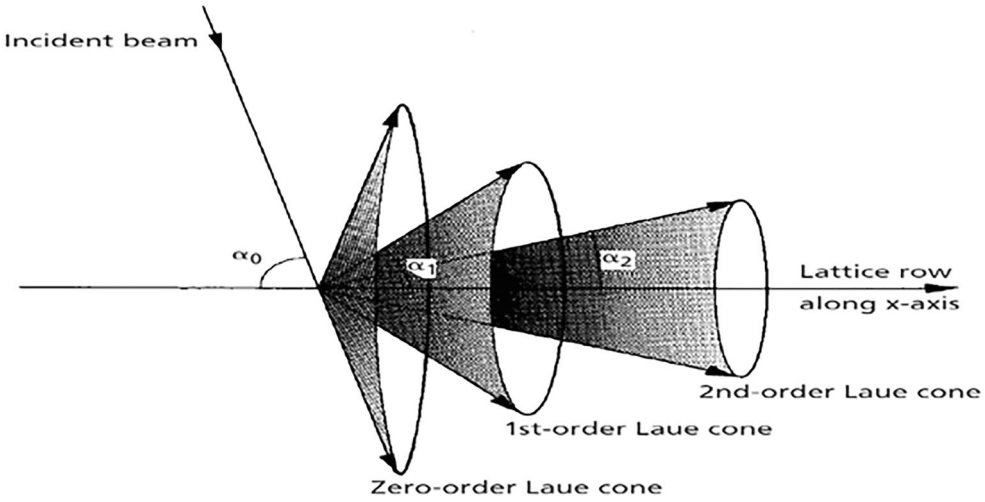

Fig. 10 Three Laue cones of diffracted beams direction from lattice row of atoms varying between 0 and 180° [33].

3.3 Ewald theory

Ewald [35] proposed a theory to explain relationship between the wavelength of light and distances of oscillators. The theory is without approximation and valid for any ratio of light wavelength to distancing oscillator. Ewald construction or sphere involves sphere of reflection and reciprocal lattice, which is used to determine if diffraction condition for reciprocal lattice point is met [33]. Consider placing a diffracting crystal at the center of Ewald sphere of 1/λ with incident beam, *I* passing through the diameter, *IO* as demonstrated in Fig. 11. The exits point of incident beam, *O* defines the origin of reciprocal lattice. If a given orientation of crystal satisfies Bragg's law for diffraction to occur, then the exit point of incident beam, *O* to exit point of diffraction beam, *B* shows vector *OB* [27, 33]. Thus, the length of the vector *OB* is equivalent to $1/d_{hkl}$ [36].

Hence, the Bragg's law is fulfilled if the reciprocal lattice point defined by reciprocal lattice vector $\boldsymbol{d}^*_{hkl}$, which correspond to reflecting planes (*hkl*) that intersect the Ewald sphere [10]. From triangle *AOC* (Fig. 11):

$$|OC| = \frac{1}{\lambda}\sin\theta = \frac{1}{2}\left|\boldsymbol{d}^*_{hkl}\right| = \frac{1}{2d_{hkl}} \tag{37}$$

The vector form of Ewald sphere to Bragg's law is given as [25, 33]:

$$\frac{(\boldsymbol{S}-\boldsymbol{S}_o)}{\lambda} = \boldsymbol{k}-\boldsymbol{k}_o = \boldsymbol{d}^*_{hkl} \tag{38}$$

where, $\boldsymbol{d}^*_{hkl}$ = reciprocal lattice vector; vector $AO = \boldsymbol{k}_o$ and vector $AB = \boldsymbol{k}$ as the origin of $\boldsymbol{d}^*_{hkl}$ shift from *A* to *O* in Fig. 11.

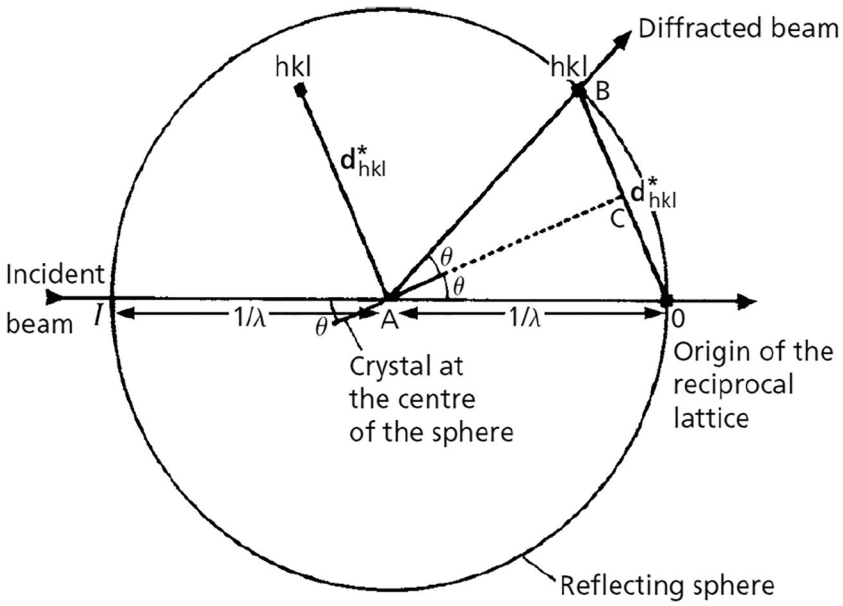

Fig. 11 Ewald sphere construction for set of planes onto diffraction position [33]

4 Diffraction application

X-ray diffraction remains a powerful technique that has long been used to solve lot of problems relating to solid crystal structures. There are wide major applications of x-ray diffraction which include phase identification, crystal size, crystal structure, residual stress/strain, dislocation density, lattice parameter determination, thermal expansion coefficient, phase transformation, and crystallographic orientation [37].

4.1 Phase identification and quantification

Every crystalline solid has a unique x-ray diffraction pattern or set of interplanar spacing and relative intensities that serves as finger print [5]. Therefore, peak positions and intensities of the diffraction of a specimen are determined and the corresponding interplanar spacings are calculated from Bragg's law. Thus, constituent phases in an unknown sample can either be identified by computerized searching from matching joint committee on powder diffraction standard (JCPDS) database that match recorded interplanar spacing values of the strongest peak intensity line, while phase quantification of unknown sample can be determined by taking peak intensities of the strongest line as a function of the weight fractions of the phases in a mixture [38].

4.2 Crystalline size

Determination of crystallite size or grain size is based on the principle that a decrease in the crystallite size leads to an increase in width of diffraction (peak broadening). Hence, an increased width is an indication that there are not enough planes in small crystallite to produce complete destructive interference [39, 40]. Debye Scherrer formulated equation for estimating particle size as [41]:

$$D = \frac{K\lambda}{B\cos\theta} \tag{39}$$

where, D= particle size, θ= angle of diffraction, K= Scherrer constant (=0.9), λ= x-ray wavelength, B= full width at half maximum (FWHM) that is measured in radian. Instrument such as detector slit width and specimen have been known to contribute to total broadening peak because of reduction in the crystallite size and strain. The specimen broadening FW(s) is described by [40]:

$$\mathrm{FW}(s)\cos\theta = \frac{K\lambda}{Size} + 4\varepsilon\sin\theta \tag{40}$$

Total broadening peak,B_t is due to specimen and instrument is given as [40]:

$$B_t^2 = \left[\frac{K\lambda}{D\cos\theta}\right] + [4\varepsilon\tan\theta]^2 + B_o^2 \tag{41}$$

where, B_o=instrument broadening and ε=strain

Williamson and Hall [42] proposed a method for deconvoluting size and strain broadening into separate equation by assuming peak width as a function of 2θ [42]:

$$B_L = \frac{k\lambda}{D\cos\theta} \tag{42}$$

$$B_e = C\varepsilon tan\theta \tag{43}$$

where, C= constant, B_L and B_e are size and strain broadening respectively. But size and strain could be convoluted if broadening peak is affected by both size and strain broadening. Therefore, Eq. (41) can be rewritten as follows:

$$B_t = B_L + B_e = C\varepsilon tan\theta + \frac{k\lambda}{D\cos\theta} \tag{44}$$

Multiplying Eq. (44) by $\cos\theta$ further yield Eq. (45):

$$B_t\cos\theta = C\varepsilon sin\theta + \frac{k\lambda}{D} \tag{45}$$

Equation (45) can be compared with a straight-line equation, $y = mx + c$. Where, m= slope and c= intercept [43]. A plot of $B_t \cos\theta$ versus $\sin\theta$ known as Williamson–Hall plot represent average grain size (slope of) component and average strain (intercept of $k\lambda/D$) component.

4.3 Crystal structure determination

Identification of crystal structure is based on lattice parameters of the unit cell of the crystal structure, lattice points, number of atoms per unit cell, packing factor of atoms in unit cell and coordinate number of atoms in the unit cell [16]. Typically, the principal diffracting planes with miller indices (h, k, l) of either all even or odd number is identified as FCC crystal structure. Whereas, the principal diffracting planes with sum of miller indices ($h + k + l$) equaling even number is identified as BCC crystal structure [28, 44].

4.4 Residual stress and strain

Stress that is left in crystal structure after removal of external force is called residual stress. Analysis of stress with x-ray diffraction techniques is based on measuring angular lattice strain distribution by measuring interplanar spacing with high diffraction peaks of sample [5]. The average internal stress is then computed from hook's law using values of strain obtained from Williamson–Hall plot or Eq. (43).

4.5 Dislocation density

X-ray diffraction peaks get equally broadened by lattice defect resulting from dislocation, which is an irregularity formed within a crystal [45]. The length of dislocation lines per unit volume of the crystal is known as dislocation density. According to Weertman [46], dislocation density increases with decreasing grain size and increasing strain. The dislocation density of a sample is estimated as [47]:

$$\delta = \frac{15B\cos\theta}{4aD} \tag{46}$$

4.6 Lattice parameters

Lattice parameters are critical variables in establishing chemical and physical properties that influence crystalline materials' state of stress and strain [10]. The six parameters (Fig. 1), which express the size and shape of crystals, called lattice parameters or unit cell parameters are length of three axes, a, b, c and corresponding angles between them, α, β, γ [12, 13]. Position of diffraction peaks are function of size and shape of the unit cell parameters while intensities of the diffraction peaks are function of atomic position in crystals. Therefore, the lattice parameters can be determined by measuring peak position over a range of 2θ from observed powder diffraction pattern and can be mathematically expressed with Bragg's law [13].

4.7 Expansion coefficient

Mechanical, optical, and electronic properties of materials at high temperature depend strongly on thermal expansion coefficient [48, 49]. High temperature x-ray diffraction technique is the most reliable method for estimating thermal expansion coefficient of materials using Rietveld analysis of powder x-ray diffraction method [50]. Intensities of diffracted beams decrease as temperature increases because atoms undergo increasing vibration around their mean position with increasing temperature [50, 51]. Therefore, values of lattice parameters vary with temperature; hence, diffraction pattern of sample can then be recorded during heating/cooling at every given temperature. Thus, polynomial models are used to express lattice parameters as a function of temperature to estimate thermal coefficient of materials [52].

4.8 Phase transformation

Phase transformation and phase diagram outline are conducted with scanning calorimetry, transmission electron microscope, nuclear magnetic, electrical resistivity, or x-ray diffraction method [53]. But, the x-ray diffraction method provides phase identity on both sides of the phase boundary. The quantity and compositional phase on phase diagram depend on heat treatment temperature, timing, and alloying content [54]. The x-ray diffraction is now widely used in phase transformation study and construction of temperature-compositional phase diagram of compound or alloying compositions by mapping out region consisting of various crystal phases [55]. Continuous recording of x-ray diffraction pattern during heating/cooling of samples allows identification of any shift of peak position owing to change in lattice constant which is a function of temperature and compositional phase [55, 56]. Therefore, the changes in diffraction patterns or peak position corresponding to phase boundary and phase(s) presence at a given temperature are then recorded accordingly [54].

4.9 Crystallographic orientation

Crystallographic orientation refers to spherical distribution of crystals in polycrystalline aggregates and may be quantified by calculating orientation distribution function, which gives orientation density as a function of rotation angle [57]. The orientation distribution function (ODF) may be calculated from pole figures either by direct inversion or series expansion method [58]. Crystallographic orientation and its distribution affect physical and mechanical properties of materials. Several engineering materials have preferred crystallographic orientation as characteristic physical and mechanical properties of material [59]. The crystallographic orientation of materials can be measured by calculating the pole figures or plotting pole figures as the stereographic projection using the rotating x-ray diffraction method [14]. Crystallographic orientation measurement should consider integration approach to sum up total diffracted intensities over an entire pole sphere and in three-dimensional diffraction pattern [57]. Randomly oriented crystals produce diffraction pattern that consist of concentric rings known as Debye–Scherrer rings if the crystals have set of crystallographic planes (h, k, l) oriented such that Bragg's diffraction condition is fulfilled. But, preferential orientation of crystals may prevent diffraction of some crystallographic planes due to how crystals are oriented [60].

5 Conclusion

This paper presented an overview of crystallographic structures, x-ray diffraction principle, and diffraction engineering applications. The review is summarized as follows:

- Nowadays, crystal structure determination and measurement of grain size, residual stress, and strain of solid metallic and non-metallic materials and many other applications are performed with automated procedure with sophisticated equipment.

- The review showed that Bragg's law provided the practical applications of x-ray diffraction to the study of crystallographic structures and major applications of x-ray diffraction. Accurate measurement of the peak position and intensities with Bragg's theory laid the foundation for crystal structure characterization.
- The wide application capabilities of x-ray diffraction were made possible by the simplified mathematical concept of Bragg's theory to measure peak positions and peak intensities. Nonetheless, the unit cell parameters of materials are more strongly dependent on peak position than peak intensity and peak width in material characterization.
- Despite wide application of x-ray diffraction, there are still misconception of few complex crystallographic structures and diffractions associated with shape of crystals. Therefore, diffraction patterns of some complex structures are inexplicable with neither Bragg nor Laue's theory.

Nomenclature α, β, γ , angle between unit cell dimensions in x, y, z directions respectively; α_n, α_o, angle between unit cell dimensions in x, y, z directions respectively; β_n, β_o, angles of diffracted and incident beams in y direction respectively; γ_n, γ_o, angles of diffracted and incident beams in z direction respectively; $\boldsymbol{r}$, crystallographic direction vector; u, v, w , crystallographic directions; δ, dislocation density; L, distance between two atoms in space; B, full width at half maximum; B_o, instrument broadening; n_1, n_2, n_3, integer numbers corresponding to wavelength; δ_{ij}, Lattice tensor; a, b, c, length of unit cell dimension in x, y, z directions respectively; h, k, l, Miller indices of crystallographic planes; D, particle size; $\boldsymbol{R}$, position lattice vectors; $\boldsymbol{a_1,a_2,a_3}$, primitive lattice vector for position vectors; $\boldsymbol{b_1,b_2,b_3}$, primitive lattice vector for reciprocal vectors; $\boldsymbol{K}$, reciprocal lattice vectors; K, Scherrer constant; B_L, size broadening; d, space distance; $\boldsymbol{d}^*_{hkl}$, space distance lattice vectors; ε, strain; B_e, strain broadening; B_t, total broadening peak; $\boldsymbol{s,s_o}$, unit vector along diffracted and incident beam directions respectively; $\boldsymbol{k,k_o}$, unit vector of reciprocal lattice along diffracted and incident beam directions respectively; λ, x-ray wavelength

References

1. Fultz B, Howe J (2013) Transmission electron microscopy and diffractometry of materials. Springer, Berlin, p 2
2. Razeghi M (2002) Fundamentals of solid state engineering. Kluwer Academic, New York, pp 5–6
3. Shackelford JF (2005) Introduction to materials science for engineers, 6th edn. Pearson Education International, London UK, p 6
4. Bhadeshia HKOH (2007) Lecture notes on x-ray and crystallographic, vol 6. Department of Material Science and Metallurgy, University of Cambridge UK, pp 11–12
5. Sharma R, Bisen DP, Shukla U, Sharma BG (2012) X-Ray diffraction: a powerful method of characterizing nanomaterials. Recent Res Sci Technol 4(8):77–79
6. Pappas N (2006) Calculating retained austenite in steel post magnetic processing using x-ray diffraction. B S Undergrad Maths Exch 4(1):8–14
7. Guma TN, Madakson PB, Yawas DS, Aku SY (2012) X-ray diffraction analysis of the microscopies of same corrosion protective bitumen coating. Int J Mod Eng Res 2(6):4387–4395
8. Hull B, John VB (1989) Non-destructive testing. Macmillan and Hound Mills Education Ltd Hampshire UK, p 5
9. Hart M (1981) Bragg angle measurement and mapping. J Cryst Growth 55:409–427
10. Fewster PF (1999) Absolute lattice parameter measurement. J Mater Sci: Mater Electr 10:175–183
11. Magner SH, Angelis RJO, Weins WN, Makinson JD (2002) A historical review of retained austenite and its measurement by x-ray diffraction. Adv X-ray Anal 45:85–97
12. Jesche A, Fix M, Kreyssig A, Meier WR, Canfield PC (2018) X-ray diffraction on large single crystals using a powder diffractometer. Phil Magaz 96(20):1–9
13. Toraya H (2016) Introduction to x-ray analysis using the diffraction method. Rigaku J 32(2):35–43
14. Zheng G, Fu T, Hengzhi F (2000) Crystal orientation measurement by xrd and annotation of the butterfly diagram. Mater Charact 44: 431–434
15. Putnam CD, Hammel M, Hura GL, Tainer JA (2007) X-Ray solution scattering (saxs) combined with crystallography and computation: defining accurate macromolecular structures, conformations and assembling in solution. Q Rev Biophys 40(3):191–285
16. Askeland DR, Fulay PP, Wright WJ (2011) The science and engineering materials, 6th edn. Cengage Learning, USA, pp 62–101
17. Dekker AJ (1952) Solid state physics. MacMillan and Co Ltd, New York, pp 6–9
18. Pierret RF, Neudeck GW (2003) Advanced semiconductor fundamentals, 2nd edn. Pearson Education Inc, USA, pp 8–14
19. Nigam GD (1987) Derivation of space group in mm2, 222 and mm crystal classes. Conference of International Atomic Agency for theoretical physics, Trieste Italy, p 5
20. Smart LE, Moore EA (2005) Solid state chemistry. Taylor & Francis Group, London, p 14–16, pp 106–108
21. Schmid E, Boas IW (1935) Plasticity of crystals. Hughes & Co. Ltd, Germany, pp 2–5
22. Hofmann P (2013) Surface physics: an introduction. Philip Hofmann, Berlin, pp 11–12
23. Kaxiras E (2003) Atomic and electronic structure. New York, Cambridge, pp 82–83
24. Muller U (2013) Symmetry relationship between crystal structures: application of crystallographic group theory in crystal chemistry. 1st edn, Oxford University Press, UK, p 25–67
25. Hammond C (2009) The basics of crystallography and diffraction, 3rd edn. Oxford University Press, UK, pp 249–255
26. Als-nielson J, Mcmorrow D (2011) Elementary of modern x-ray physics, 2nd edn. John & Wiley, UK, pp 153–157
27. Wood EA (1964) Vocabulary of surface crystallography. J Appl Physiol 35(4):1306–1312
28. Tilley R (2004) Understanding of solid: the science of materials. Willey & Sons Ltd, West Sussex, p 138
29. Ibach H (2009) Solid state physics: an introduction to principle of material science, 4th edn. Springer, pp 20–25
30. Zhang Y, Colella R, Kycia S, Goldman AI (2002) Absolute structure-factor measurement of al-pd -mn of quasicrystal. Acta Cryst A 58:385–390
31. Authier A (2002) Dynamical theory of x-ray diffraction. Acta Cryst (A) 58:12–414
32. Sivia DS (2011) Elementary scattering theory for x-ray and neutron users. Oxford University Press, pp 7–New York, 10
33. Hammond C (2001) The basics of crystallography and diffraction, vol 137, 2nd edn. Oxford University Press, New York, pp 194–197
34. Ashcroft NW, Mernin ND (1976) Solid state physics. HRW International Edition. Asian Ltd, Singapore, pp 5–7
35. Ewald PP (1912) To find the optical properties of an anisotropic arrangement of isotropic oscillator. Ph.D Thesis, Institute of Theoretical Physics, University of Munich Germany

36. Fewster PF (2018) Response to Fraser & Wark's comments on a new theory for x-ray diffraction. Acta Cryst A74:457–465
37. Winter C (2000) Efficiently optimizing manufacturing processes using iterative taguchi analysis. Lambda Research Inc, Diffraction note, No25 p 1-4
38. Gilmore CJ, Barr G, Paisley L (2004) High throughput powder diffraction. A new approach to qualitative and quantitative powder diffraction pattern analysis using full pattern profile. J Appl Cryst 37:231–242
39. Barman B, Sarma KC (2010) Structural characterization of PVA capped ZnS nano structured thin film. India J Phys 86(8):703–707
40. Jacob R, Nair HG, Isac (2015) Structural and morphological studies of nano-crystalline ceramic BaSro.9Feo.TiO4. Int Lett Chem Phys Astron 44:15–107
41. West AR (1974) Solid state chemistry and its application. Wiley & Sons, New York, p 27
42. Williamson GK, Hall WH (1953) X-ray line broadening from field aluminum and wolfram. Acta Metall 40(1):22–31
43. Vinila VS, Jacob R, Mony A, Nair HG, Isaa S, Rajan S, Nair AS, Isac J (2014) XRD studies on nano crystalline ceramic superconductor PbSrCaCuo at different treating temperature. Cryst Struct Theory Appl 3:1–9
44. Henry NF, Lipson H, Wooster WA (1961) The interpretation of x-ray diffraction photographs. Macmillian Ltd, London, p 33
45. Ungar T (1994) Strain broadening caused by dislocation. Mat Sci Forum 923:166–169
46. Weertman JR (1993) Hall-Petch strengthening in nano crystalline metals. Mater Sci Eng A166:161–167
47. Subbaiah YPV, Prathap P, Reddy KTR (2006) Structural, electrical and optical properties of ZnS film deposited by close- spaced evaporation. Appl Surf Sci 253(5):2409–2415
48. Hummer DR, Heaney PJ, Post JE (2007) Thermal expansion of anatase and rutile between 300 and 575k using synchrotron powder x-ray diffraction. Powder Diffract 22(4):352–356
49. Huang C, Hsu Y, Chen J, Suryanarayanan V, Lee K, Ho K (2006) The effects of hydrothermal temperature and thickness of TiO_2 film on the performance of a dye-sensitized solar cell. Solar Energy Mater Sol 90:2391–2397
50. Nagash S, Gerhards MT, Tietz F, Guillon O (2018) Coefficient of thermal expansion of Al and Y-substituted NaSICON solid solution $Na_{3+2x}Al_xY_xZr_{2-2x}Si_2PO_{12}$. J Batter 4(33):1–9
51. Pathak PD, Vasavada NG (1970) Thermal expansion of nacl, KCl and CSBr by x-ray diffraction and the law of corresponding states. Acta Cryst A26:655–661
52. Jagtap N, Bhagwat M, Awati P, Ramaswamy V (2005) Characterization of nanocrystalline anatase titania: an in-situ HTXRD study. Thermochimica Acta 427(1 -2):37–41
53. Lekston Z, Zubko M (2016) X-ray diffraction studies of the reversible phase transformation in niti shape memory alloy. Acta Phys Polon A 130(4):1059–1062
54. Pederson R (2002) Microstructure and phase transformation of Ti-6AL-4V. MSc Thesis, Lulea University of Technology, Sweden
55. Caffrey M, Hing FS (1987) A temperature gradient method for lipid phase diagram construction using time-resolve x-ray diffraction. J Biophys Soc 51:37–46
56. Malinov S, Sha W, Guo Z, Tang CC, Long AE (2002) synchrotron x-ray diffraction study of the phase transformation in titanium alloys. Mater Charact 48:279–295
57. Jia J, Raabe D (2006) Evolution of crystallinity and crystallographic orientation in isotactic polypropylene during rolling and heat treatment. Eur Poly J 42:1755–1766
58. Cleton F, Jouneau PH, Henry S, Gaumann M, Buffat PA (1999) crystallographic orientation assessment by electron backscattered diffraction. Scanning 21:232–237
59. Connolly JR (2012) Introduction to X-ray powder, Research note, EPS 400-001, p 10
60. Alejandro BR (2007) Fast quantification of avion eggshell microstructure and crystallographic texture using two-dimension x-ray diffraction. Br Poult Sci 48(2):133–144